The Observable Field in Complex Scattering Scenarios

Neto, Andrea; Fiorellini Bernardis, Arturo; Emer, Diego; Freni, F.; Llombart, Nuria

DOI
10.1109/TAP.2020.2978885

Publication date
2020

Document Version
Accepted author manuscript

Published in
IEEE Transactions on Antennas and Propagation

The Observable Field in Complex Scattering Scenarios

Andrea Neto, *Fellow, IEEE*, Arturo Fiorellini Bernardis, Diego Emer, Angelo Freni, *Senior Member, IEEE*, and Nuria Llombart, *Senior Member, IEEE*

***Abstract*— The Observable Field is defined as the portion of the incident field that can contribute to the power received by an antenna. Recently, the Observable Field was estimated for a plane wave incidence. Here, the procedure is extended to a general incident field expressed as a superposition of homogeneous plane waves. The Observable Field concept provides a methodology to evaluate the maximum power that could be received by an ideal terminal antenna. In particular, it emerges that to maximize the received power, the pattern in transmission of the antenna should be synthesized to reproduce the angular pattern of the Observable Field. This is specifically relevant in cases of non-line of sight at high frequencies, where the power received can drop by orders of magnitude. As a case study, we consider a communication scenario which involves a base station and distributed receivers embedded in a complex scattering environment.**

***Index Terms*—Antennas, reception, equivalent circuit**

I. Introduction

The definition of the power available to an antenna illuminated by a plane wave has been extensively discussed in the literature [1]-[4] and it is still a relevant research topic [5]-[7]. Nowadays, there are many applications, such as wireless communications, radar systems, automotive applications, where the receiving antenna is immersed in a complex environment, and the incident field cannot be represented with a single plane wave. In such complex scenarios it could be very useful to a priori understand what could be the maximum power that can be theoretically received by a lossless antenna. In fact, this knowledge allows us to evaluate the margin of improvement that could be expected when a complex antenna system is exploited.

For this purpose, we propose a generalization of the Observable Field methodology already introduced in [7] for a single plane wave incidence. There the Observable Field was defined as the portion of a single incident plane wave that can contribute to the signal received by an antenna filling a fixed volume (a sphere of radius a). The Observable Field was obtained by removing from the incident field the portion that provides negligible contributions to the received signal, i.e. the remaining field, $\vec{e}_{rem}(\vec{r})$, as follows:

$$\vec{e}_{obs}(\vec{r}) = \vec{e}_i(\vec{r}) - \vec{e}_{rem}(\vec{r}). \quad (1)$$

In particular, for a given incident plane wave with electric field, $\vec{e}_i$, the angular distribution of the Observable Field was constructed in [7] as the radiation from the equivalent currents radiating the incident field behind the antenna, but truncated on a disk, with diameter equal to the minimum sphere enveloping the antenna, orthogonal to the direction of propagation. The angular distribution was multiplied by a specific constant, that can be calculated analytically, ensuring that the Observable Field carries the available power that an ideal antenna can receive, even in the case of electrically small antenna domains. For a complex incident field distribution, the field can be first expressed as a continuous superposition of homogeneous plane waves. Then, a procedure similar as that described in [7] can be applied, where the equivalent currents distributions are calculated as coherent superposition of those obtained for each component of the homogeneous plane wave spectrum distributed now on a spherical domain. The amplitude of the Observable Field cannot anymore be evaluated analytically, but numerically via field reaction integrals.

As relevant example of application of the proposed methodology, terminal antennas for 5G [8] or for further generations communication systems are discussed. In complex scattering scenarios, the optimal terminal antenna that maximize the received power is an open research question [9], [10]. In particular, in high frequency wireless links, the receiving terminal can be a phased array antenna with beam shaping capabilities [9], [11] - [13] to overcome limitations due to possible absence of a line of sight (LOS) link [14]. The terminal antenna should be steered towards the base station (LOS link) or towards strong nearby reflecting objects (NLOS link). Moreover, for mm-waves links, the terminal antenna could also exploit beam shaping capabilities to ensure the link from near-by objects, as shown in the scenario described in this contribution.

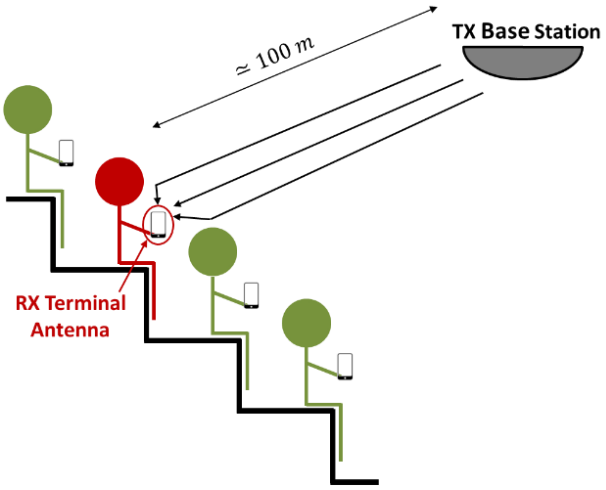

Fig. 1 Stadium scenario: geometry, including the base station, and main scattering contributions.

To derive the optimal beam shape which maximizes the received signal, it is convenient to analyse the propagation channel in downlink. This is because the base station antenna provides a predictable field, independently from the position and orientation of each specific terminal. Thus, the incident

field on the mobile terminal needs to be evaluated just once, as for example in the stadium scenario depicted in Fig. 1. In such scenario, we imagine tens of thousands of users each one carrying a mobile terminal antenna receiving a signal coming from a transmitting base station located, in the centre of the stadium at about 100 m. For such scenario, a possible 120 GHz architecture, based on a line of sight power budget analysis to provide on-demand coverage, was proposed in [15].

Here, a carrier frequency of 120 GHz is investigated. The dominant contribution to the Observable Field is typically given by the LOS signal; however, contributions emerging from the main near-by scatterers (reflected, transmitted and diffracted rays) are also clearly identifiable, and thus can be driving the synthesis of the reception beams when the LOS is not the dominant term.

Section II shows the derivation of the Observable Field for an arbitrary incident field distribution by means of the ideal currents. In Section III, we calculate the maximum power received by the ideal antenna operating in reception starting from the Thevenin equivalent circuit representation. In Sections IV and V, we apply the procedure to the case of a terminal antenna embedded in the complex stadium scenario illuminated by a generic incident field. Finally, we discuss the conclusions in Section VI.

II THE OBSERVABLE FIELD FOR GENERALIZED INCIDENCE

In this section, we propose a procedure to derive the Observable Field for an antenna, located inside a spherical domain S_a of radius a, when it is illuminated by an arbitrary incident field. The Observable Field allows us to evaluate the maximum power that can be received by the antenna. In the literature different procedures have been suggested to evaluate such maximum power for a single plane wave incidence [1]-[3], [7]. Here, we generalize the procedure described in [7] to an arbitrary illumination.

For a general source distribution, the incident electric field, defined in absence of the antenna, can be expressed as a continuous superposition of homogeneous plane waves referred to the reference system located in the antenna domain, as:

$$\vec{e}_i(\vec{r}_a) = \int_0^{2\pi}\int_0^{\pi} \vec{E}_i^{\,pws}(-\hat{k}_i)e^{jk\vec{r}_a\cdot\hat{k}_i}\, d\hat{k}_i, \qquad (2)$$

where $\vec{r}_a$ identifies an observation point on the antenna domain, $\hat{k}_i = sin\beta_i cos\alpha_i\hat{x} + sin\beta_i sin\alpha_i\hat{y} + cos\beta_i\hat{z}$, $\vec{E}_i^{\,pws}$ is the electric field plane wave spectrum associated to the incident field, and $-\hat{k}_i$ is the direction of propagation of each plane wave. The associated magnetic field spectrum can be evaluated as $\vec{H}_i^{\,pws} = -\hat{k}_i \times \vec{E}_i^{\,pws}/\zeta$, with ζ being the free space characteristic impedance. The integral in (2) is parametrized with $\beta_i \in (0,\pi), \alpha_i \in (0,2\pi)$ and $d\hat{k}_i = sin\beta_i d\beta_i d\alpha_i$. The derivation of the plane wave spectrum, $\vec{E}_i^{\,pws}$, from the knowledge of the incident electric and magnetic fields on a sphere with radius $R_f > a$ enclosing the antenna domain, is shown in Appendix A, for the sake of completeness.

Similarly, as in [7], the Observable Field is defined in the far field of the antenna domain, $\vec{r}_\infty$, as the product of a normalized spherical wave, $\vec{f}_{po}(\vec{r}_\infty)$, and the amplitude, C:

$$\vec{f}_{obs}(\vec{r}_\infty) \approx C\vec{f}_{po}(\vec{r}_\infty), \qquad (3)$$

where, for convenience, we used a notation that combines the electric and the magnetic fields in a unique vector:

$$\vec{f}(\vec{r}) = \begin{bmatrix}\vec{e}(\vec{r})\\ \vec{h}(\vec{r})\end{bmatrix}. \qquad (4)$$

Both the amplitude, C, and the angular distribution, $\vec{f}_{po}$, are functions of the incident field and the antenna domain S_a via its radius a. The amplitude C ensures that the observable field carries the available power that the ideal antenna can receive. This amplitude tends to unity for electrically large antenna domains, while it grows for $a/\lambda \to 0$. For each plane wave component of the spectrum in (2), the field scattered by the ideal receiving antenna can be approximated [7] by using surface currents, $\vec{J}_{po}(\hat{k}_i,\vec{r}_a), \vec{m}_{po}(\hat{k}_i,\vec{r}_a)$, defined over the antenna domain, and evaluated by using a Physical Optics (PO) approximation. The angular distribution $\vec{f}_{po}$ can then be derived from the field radiated by the superposition of all the current distributions (one for each component of the homogeneous plane wave spectrum of the incident field).

More specifically, the electric and magnetic fields in the right-hand side of (3) can be expressed as the sum of an inward and an outward propagating spherical waves, as follows:

$$\vec{e}_{po}(\vec{r}_\infty) = \left[\vec{V}_{po}^{inw}(\hat{k})\frac{e^{jkr_\infty}}{r_\infty} + \vec{V}_{po}^{outw}(\hat{k})\frac{e^{-jkr_\infty}}{r_\infty}\right] \qquad (5a)$$

$$\vec{h}_{po}(\vec{r}_\infty) = -\frac{1}{\zeta}\hat{k}\times\vec{e}_{po}^{inw}(\hat{k}) + \frac{1}{\zeta}\hat{k}\times\vec{e}_{po}^{outw}(\hat{k}) \qquad (5b)$$

where $\hat{k} = sin\theta cos\phi\hat{x} + sin\theta sin\phi\hat{y} + cos\theta\hat{z}$ and $\vec{V}_{po}^{inw}(\hat{k}) = \vec{V}_{po}^{outw}(-\hat{k})$. In (5) the factorization of the inward and outward waves separates the angular (θ,ϕ) dependency of the Observable Field from the radial dependence (r_∞).

I.1 Angular Distribution of the Observable Field

In [7], it was proposed that the outward angular distribution, $\vec{V}_{po}^{outw}(\hat{k})$, of the Observable Field related to an ideal antenna illuminated by a single plane wave, $-\hat{k}_i$, could be evaluated as the field radiated by uniform surface currents, $\vec{J}_{po}(\hat{k}_i,\vec{r}_a), \vec{m}_{po}(\hat{k}_i,\vec{r}_a)$, defined over the disk $S_a(\hat{k}_i)$ of radius a, defined in Fig. 2, orthogonal to the plane wave direction of propagation. The currents over the disk can be seen as a spatial truncation of the equivalent currents that will describe the plane wave incident field in the half space below the disk (i.e. $\vec{r}\cdot\hat{k}_i < 0$ in Fig. 2). An ideal antenna operated in reception should scatter a field, $\vec{e}_{scat}$ which is equal but opposite to the outward propagating wave of the Observable Field, $\vec{e}_{scat}(\vec{r}_\infty) = -C\vec{e}_{po}^{outw}(\vec{r}_\infty)$, cancelling it out. In other words, the ideal antenna absorbs the entire inward propagating power of the Observable Field.

It can be shown that the equivalent currents, evaluated over the disc or over a half spherical surface that is bounded by the

same disk (see Fig. 2), radiate the same field in $\vec{r}\cdot\hat{k}_i<0$. The advantage of expressing the currents on the sphere S_a rather than on the disk is that, when multiple plane waves are combined, an effective total current emerges as the sum of all contributions over a continuous surface.

Generalizing to any incident plane wave direction, $-\hat{k}_i$, the chosen hemispherical surface, where to distribute the equivalent currents, faces the direction of origin of the plane wave, i.e. $\hat{r}_a\cdot\hat{k}_i>0$, (top sphere). Therefore, the appropriate set of PO currents over the entire spherical domain S_a can be expressed as follows:

$$\vec{J}_{po}(-\hat{k}_i,\vec{r}_a)=\begin{cases}-\hat{r}_a\times\vec{H}_i^{\,pws}(-\hat{k}_i)e^{jk\vec{r}_a\cdot\hat{k}_i} & \forall\,\vec{r}_a\cdot\hat{k}_i>0\\ 0 & \forall\,\vec{r}_a\cdot\hat{k}_i<0\end{cases}, \tag{6a}$$

$$\vec{M}_{po}(-\hat{k}_i,\vec{r}_a)=\begin{cases}\hat{r}_a\times\vec{E}_i^{\,pws}(-\hat{k}_i)e^{jk\vec{r}_a\cdot\hat{k}_i} & \forall\,\vec{r}_a\cdot\hat{k}_i>0\\ 0 & \forall\,\vec{r}_a\cdot\hat{k}_i<0\end{cases}. \tag{6b}$$

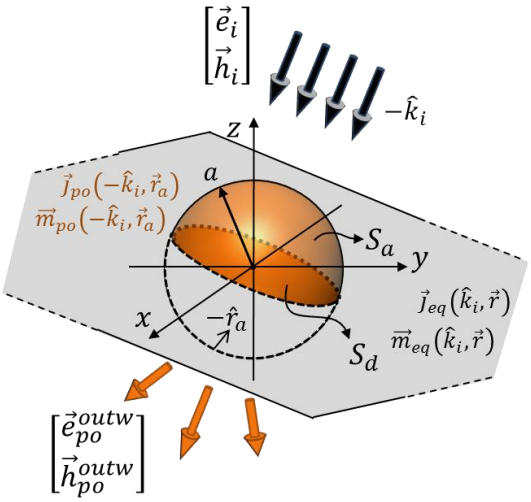

Fig. 2 Geometrical definition of the domains where the PO currents $\vec{J}_{po},\vec{M}_{po}$ and the equivalent currents $\vec{J}_{eq},\vec{M}_{eq}$ are distributed in the case of a single plane wave impinging from $-\hat{k}_i$. The equivalent currents, defined over a plane orthogonal to $\hat{k}_i$ (highlighted in grey), plus those defined on the disk S_d or on the top hemisphere of S_a, represent the incident field in the half space $\vec{r}\cdot\hat{k}_i<0$. The PO currents are the equivalent currents truncated over the antenna domain (highlighted in orange): either the disk S_d or the top hemisphere of S_a.

The angular distribution of the outward component of the observable field, $\vec{e}_{po}^{\,outw}$, can be then calculated as the radiation from a continuous summation of the currents distributions in (6) related to each homogenous plane wave components of the incident field spectrum, as follows:

$$\vec{J}_{po}(\vec{r}_a)=\int_0^{2\pi}\int_0^{\pi}\vec{J}_{po}(-\hat{k}_i,\vec{r}_a)\,d\hat{k}_i, \tag{7}$$

$$\vec{M}_{po}(\vec{r}_a)=\int_0^{2\pi}\int_0^{\pi}\vec{M}_{po}(-\hat{k}_i,\vec{r}_a)\,d\hat{k}_i\,. \tag{8}$$

Fig. 3 gives a graphical example of how these ideal currents are generated in a point Q of the spherical surface S_a of coordinate $\vec{r}_a$. In particular, only the inward portion of the incident field spectrum for which $\vec{r}_a\cdot\hat{k}_i>0$ contributes to the equivalent currents in Q.

The spherical surface S_a, was taken here for the sake of simplicity, however any closed surface bounding the antenna could be chosen and the proposed procedure could be easily extended, following the same PO approximation.

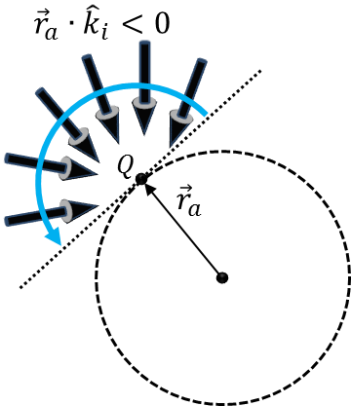

Fig. 3 Inward plane waves contributing to the PO currents in an arbitrary point Q of the spherical surface S_a.

For the sake of clarity, Fig.4 shows the ideal electric currents due to different combinations of plane waves impinging from the $z>0$ half space and propagating along the z,x plane. Fig. 4a shows the magnitude of the x component of the equivalent electric current distribution $\vec{J}_{po}$ on the sphere S_a for the case of a single plane wave coming from broadside, $\beta_i=0$, whose electric field is linearly polarized along $\hat{x}$. The antenna spherical domain radius has been set to $a=\lambda_0$. The currents are distributed only on the upper half of the sphere. Fig. 4b and 4c show the magnitude of the x component of the equivalent electric currents $\vec{J}_{po}$ in case of two plane waves coming from directions $\beta_i=\pm15^o$ and polarized as shown in the figures inset. Fig. 4b is pertinent to two plane waves whose electric field sum in-phase at the origin (referred as *in-phase* configuration) whereas Fig. 4c corresponds to the out of phase summation (referred as *out-phase* configuration). For these configurations, the currents remain relevant only on the top sphere. Finally, Fig. 4d and 4e show similar quantities but for two plane waves coming from directions $\beta_i=\pm55^o$. In these cases, the ideal currents are relevant also on the bottom sphere.

It is worth noting that for more realistic cases where the field spectrum is continuous no discontinuities will be observed for the current distributions, unlike for these simplified examples.

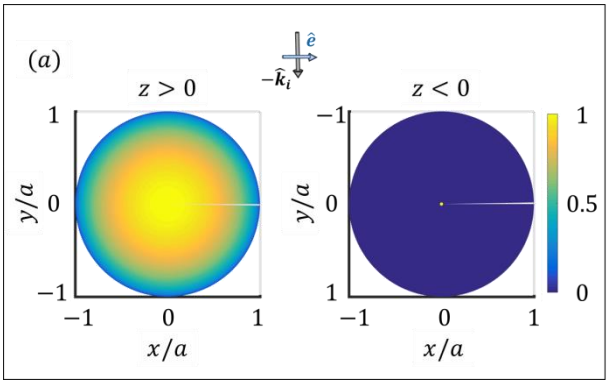

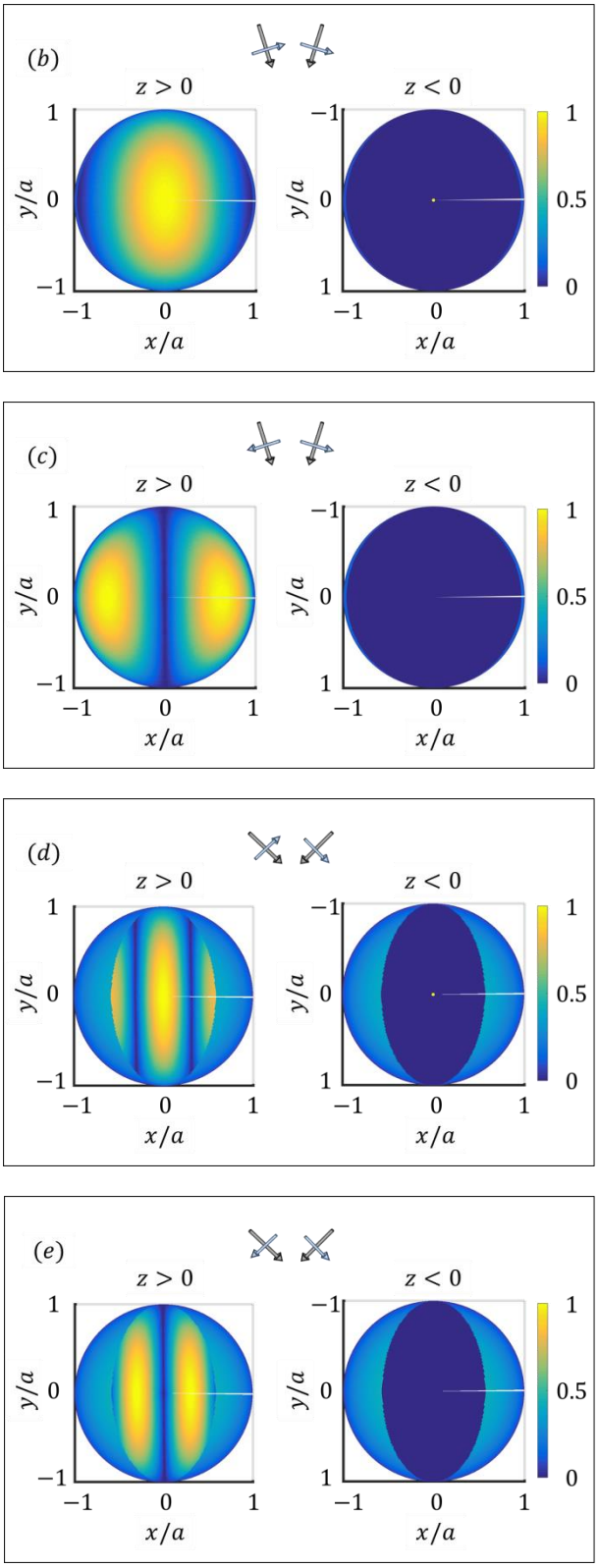

Fig. 4 Normalized magnitude of the x-component of the ideal electric currents $|\vec{J}_{eq,x}|/\max|\vec{J}_{eq,x}|$ (top-hemisphere $z > 0$ to the left, bottom-hemisphere $z < 0$ to the right), for the plane wave configurations sketched in the inset of each figure: single plane wave coming from broad side (a), two plane waves coming from $\beta_i = \pm 15^o$ with *in-phase* (b) and *out-phase* (c) configurations, and $\beta_i = \pm 55^o$ with *in-phase* (d) and *out-phase* (e) configurations.

The far field outward distributions of the observable fields corresponding to the *in-phase* and *out-phase* plane wave configurations of Fig. 4b and 4c are shown in Fig. 5a and 5b, respectively. Three different antenna domain radii are now investigated. It is apparent that for large radii in terms of wavelength, the *in-phase* and *out-phase* outward Observable Field patterns are similar and are both characterized by two distinct beams related to the direction of the incident waves. Conversely, for electrically small radii, the plane wave configuration makes a significant difference in the pattern of the Observable Field. Note that for small radii, due to the low directivity, the Observable Field tends to reproduce a Huygens' pattern for the *in-phase* case.

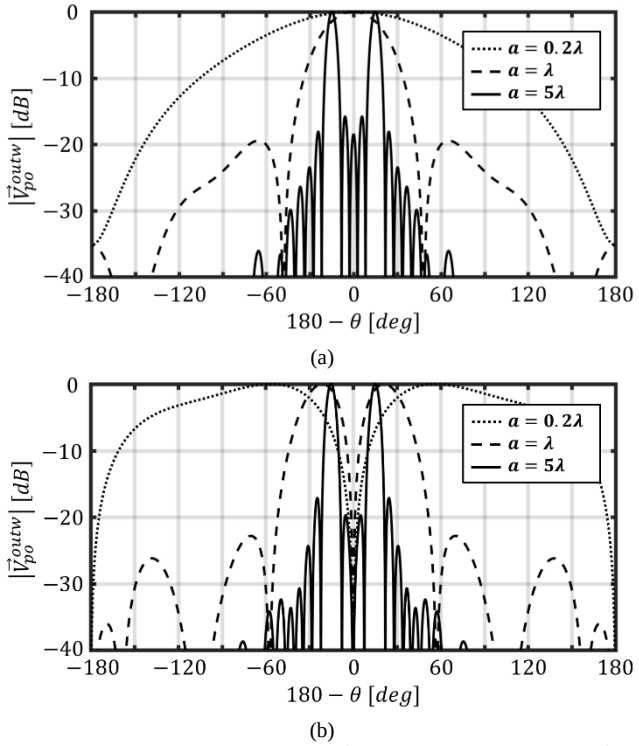

Fig. 5 Normalized magnitude plots of the outward component of the Observable Field predicted by the Ideal Current procedure for three different antenna radii when two plane waves are impinging from $\beta_i = \pm 15°$ for the *in-phase* (a) and *out-phase* (b) configurations.

II.2 Amplitude of the Observable Field

The amplitude C of the Observable Field was given analytically in [7] for a single plane wave. In case of a generalized incident field, this amplitude depends on the superposition of all the plane wave components and has to be evaluated numerically. To this purpose, the Observable Field in (3) can be thought as the product of a single basis function, $\vec{f}_{po}$, and its associated amplitude, C. Appendix B clarifies how this amplitude can be approximated resorting to the reciprocity reaction integral between the incident field and the field radiated by the ideal antenna, as follows:

$$C \approx \frac{\langle \vec{f}_i, \vec{f}_{tx} \rangle}{\langle \vec{f}_{po}, \vec{f}_{tx} \rangle}, \tag{9}$$

where the reaction integral between two generic basis $\vec{f}_b = \begin{bmatrix} \vec{e}_b \\ \vec{h}_b \end{bmatrix}$ and test $\vec{f}_t = \begin{bmatrix} \vec{e}_t \\ \vec{h}_t \end{bmatrix}$ functions is taken as follows:

$$< \vec{f}_b, \vec{f}_t > \equiv \iint_{S_\infty} \left[\frac{1}{\zeta} \vec{e}_b(\vec{r}) \cdot \vec{e}_t(\vec{r}) - \zeta \vec{h}_b(\vec{r}) \cdot \vec{h}_t(\vec{r}) \right] d\vec{r}. \tag{10}$$

The integration in (10) is performed on a spherical surface, S_∞, located in the far field of the antenna. In (9) $\vec{f}_i$ is the field

vector associated to the incident field, while $\vec{f}_{tx}$ is the field vector associated to the fields radiated by the ideal antenna when operating in transmission (for more details refer to Appendix B).

Fig. 6 shows the value of the amplitude constant C for the same incident field cases of Fig. 5 as function of the antenna domain radius. It can be seen that for electrically large domains, where the scattered field by the PO currents represents well the incident field in the region behind the antenna, the amplitude constant tends to unity, and a field picture similar to that of the penumbra region in large objects is achieved [4]. In this case, the power received by the ideal antenna under a single plane wave can be represented with an effective area tending to its physical area [7]. Instead, the amplitude C grows for $a/\lambda \to 0$ compensating the fact that the physical area tends to zero.

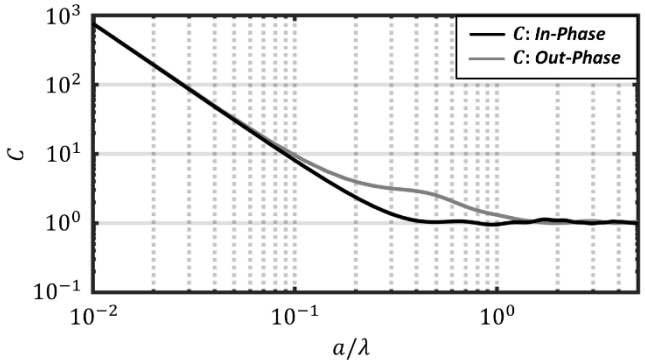

Fig. 6 Value of the amplitude constant C as a function of the antenna dimension in case of two plane waves incoming from $\beta_i = \pm 15$ for the *in-phase* and *out-phase* configurations described in Fig. 4b and c, respectively. Check oscillations

III ESTIMATIONS OF THE AVAILABLE POWER

Using the Thevenin equivalent circuit, the power received by a matched antenna can be expressed in terms of its open circuit voltage, V_{oc}, and its radiation resistance, R_{rad}, as follows:

$$P_{rec} = \frac{|V_{oc}|^2}{8R_{rad}} = \frac{|V_{oc}I_0|^2}{16P_{rad}^{tx}(I_0)}. \quad (11)$$

where the radiation resistance is expressed in terms of the power $P_{rad}^{tx}(I_0)$ radiated by the same antenna assuming I_0 as the value of the current flowing into the antenna terminals when operating in transmission. It is known that $V_{oc}I_0$ can be expressed as a reaction integral [16], [17] on the surface of a sphere S_∞ at large distance from the antenna, as follows

$$V_{oc}I_o = \iint_{S_\infty}\left[\vec{e}_{tx}(\vec{r}) \times \vec{h}_i(\vec{r}) - \vec{e}_i(\vec{r}) \times \vec{h}_{tx}(\vec{r})\right] \cdot \hat{r}\, d\vec{r}\,, \quad (12)$$

where $\vec{e}_i, \vec{h}_i$ is the incident field in absence of the antenna and $\vec{e}_{tx}, \vec{h}_{tx}$ are the fields radiated by the antenna when operated in transmission. For the ideal antenna, these fields are those radiated by the currents $\vec{J}_{tx}(\vec{r}_a), \vec{m}_{tx}(\vec{r}_a)$ defined in (B3a) and (B3b). The amplitude of these currents is proportional to I_0 which value is, however, not relevant for calculating the received power in (11).

Since the fields evaluated in (12) are in the far field region of the antenna $\vec{h}_{tx} = \frac{1}{\zeta}\vec{r} \times \vec{e}_{tx}$, and (12) can be re-written as follows:

$$V_{oc}I_0 = \iint_{S_\infty}\left[\frac{1}{\zeta}\vec{e}_{tx}(\vec{r}) \cdot \vec{e}_i(\vec{r}) - \zeta \vec{h}_{tx}(\vec{r}) \cdot \vec{h}_i(\vec{r})\right] d\vec{r} = \\ = \langle \vec{f}_i, \vec{f}_{tx} \rangle\,, \quad (13)$$

which can be recognized as the reaction integral in (10).

On the other hand, as demonstrated in Appendix B, the power radiated by the ideal antenna in transmission can also be expressed in terms of a reaction integral as $P_{rad}^{tx} = \frac{1}{4}\langle \vec{f}_{po}, \vec{f}_{tx} \rangle$. Accordingly, by using eq. (11) and (13), the available power to any antenna bounded by the surface S_a can be expressed as follows:

$$P_{avail} = \frac{|\langle \vec{f}_i, \vec{f}_{tx} \rangle|^2}{4\langle \vec{f}_{po}, \vec{f}_{tx} \rangle}. \quad (14)$$

Finally, by using the expression of the Observable Field (3) and the approximation of its amplitude (9), the available power becomes equal to the inward (or the outward) power associated to the Observable Field:

$$P_{avail} = \frac{|C|^2\langle \vec{f}_{po}, \vec{f}_{tx} \rangle}{4} = P_{inw} = P_{outw} \quad (15)$$

where $P_{inw/outw} = |C|^2 \iint_{S_\infty} \left|\vec{e}_{po}^{\,inw/outw}(\vec{r})\right|^2 / 2\zeta d\vec{r}$.

It is worth noting that the calculation of the Observable Field constant, C, as defined in (9), can be costly from a numerical point of view, given the fact that the incident field is characterized by fast oscillations when projected on a sphere of large radius in terms of wavelength. This is a typical situation in many scattering problems. To this regard, resorting to the reciprocity Theorem, the field reaction $\langle \vec{f}_i, \vec{f}_{tx} \rangle$ in (13), which also appears in the numerator of (9), can be performed over the antenna domain sphere, S_a, as follows:

$$\langle \vec{f}_i, \vec{f}_{tx} \rangle = \iint_{S_a}\left(\vec{J}_{tx} \cdot \vec{e}_i - \vec{m}_{tx} \cdot \vec{h}_i\right) d\vec{r}_a\,. \quad (16)$$

The evaluation of this reaction is more efficient as the oscillations of the incident fields are much slower than in (13). An application domain in which (16) is particularly appropriate is detailed in Section IV, which introduces a complex communication scenario.

To clarify the meaning of the available power under the incidence of multiple plane waves, it is useful to investigate the same cases described in Figs. 5 and 6 of two incident plane waves with unitary electric field magnitude. Fig. 7 shows the available power, normalized to the one obtained from a single incident plane wave with unitary electric field magnitude impinging from $\beta_i = 0$, as a function of the antenna radius a. The dashed lines shows the results evaluated using the proposed procedure for both *in-phase* and *out-phase* configurations. For small antenna radii the curves pertinent to the *in-phase* field configuration start from values close to 4, indicating an almost coherent summation of the field contributions. The *out-phase* curves, starting almost from zero, indicate an almost complete cancellation. For larger radii, the outward Observable Field tends to reconstruct two completely independent beams, pointing toward $\theta = 180^o \pm 15^o$, as shown in Fig. 5. Accordingly, the total available power remains equal to twice the contribution of

each plane wave when considered individually. For this scenario, there is no qualitative difference between the *in-phase* and *out-phase* cases, and the power density carried by each incident plane wave is summed incoherently. In the same figure, a comparison between the available power calculated by using a spherical modes representation, as suggested by [5], is also reported. As in the case of a single plane wave described in [7], the quantized nature of the spherical wave expansion emerges clearly; however, the curves, obtained using both the Spherical Modes and the Ideal Currents procedure, are qualitatively equivalent for larger antenna radii, where the discretization error becomes negligible.

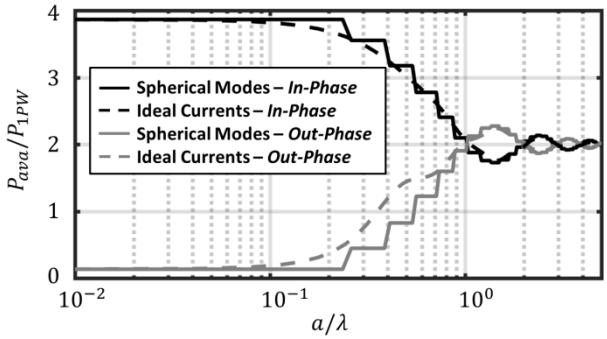

Fig.7 Available power versus antenna domain radius for two plane waves, with unitary electric field magnitude and impinging from $\beta_i = \pm 15°$, normalized to the available power obtained for a single plane wave having the same magnitude. Comparison between ideal currents (solid) and $N = \lceil ka \rceil$ spherical modes (dash) procedures.

IV THE STADIUM SCENARIO

With reference to Fig.1 a stadium with tens of thousands of spectators is considered equipped with a wireless system as described in [15]. The wireless link to the spectators is provided via a centrally positioned base station (assumed for simplicity to be at a distance of 100 m from the investigated spectator). A carrier frequency of $f = 120$ GHz is considered. A radiated power of $P_t = 14$ dBm is transmitted in each beam that the base station generates independently. The gain of the base station antenna is characterized by an effective area at of $G_t\lambda^2/(4\pi) = 12.5$ cm^2. At the envisioned high frequencies scenario, the base station generates thousands of narrow independent beams, each covering a small angular cell that hosts ≈ 50 spectators.

In the present example, the line of sight (LOS) field reaches the spectator with an angle of $\theta_{BS} = 0^o$ with respect to the horizon (see Fig.8) and a linear polarization along $\hat{y}$. To obtain a complete description of the incident fields on the terminal antenna, the LOS contribution must be complemented by the field scattered by the surroundings. The schematic representation of the scatterers around the investigated terminal antenna is shown in Fig.8: they are the head and the torso of the spectator under analysis, and the head of the spectator in front. All of these objects are modelled as thick dielectrics, with a complex relative permittivity of $\varepsilon_r = 6 - j6$ at 120 GHz [18]. The surface of the scatterers is considered rough. The torso has a rms of 1 mm, and a correlation length of 3.5 cm along x and of 5 cm along y, whereas the heads have a rms of 4.7 mm, and a correlation length of 7 cm along x and of 6 cm along y. A Physical Optics tool (GRASP, [19]) is used to calculate the scattered field.

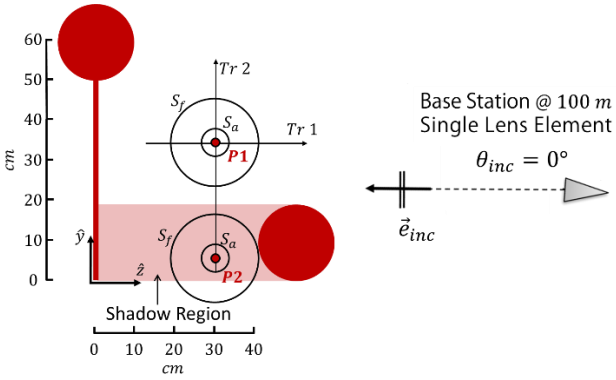

Fig.8 Geometry of the problem relevant to the area surrounding the user terminal antenna. Chosen reference system aligned with the direction of incidence of the LOS field. In red are the main scatterers: head and torso of the user under analysis, and head of the user in front. The red dots, P_1, P_2, indicate the two points where the Observable Field is evaluated. S_a indicates the antenna domain (sphere of radius $a = 3.5$ mm), while S_f is the surface used to calculate the incident field spectrum (in this case $R_f = 7cm$). $Tr\ 1$, $Tr\ 2$ indicates the reference system used to evaluate the incident field maps and received power.

The incident field on the surroundings of the antenna terminal is shown in Fig. 9 at 120 GHz. The visible interference pattern with the LOS field is given by the reflection from the torso, which does not scatter a plane wave due to the rough surface. Moreover, the head of the neighbouring spectator creates a shadow region with respect to the LOS field from the base station.

Let us consider a terminal antenna characterized with an Airy pattern of 19 dB directivity. This corresponds to the ideal antenna for a single plane wave in a sphere of radius 3.5 mm as described in [7]. Fig. 10 shows the received power by this antenna oriented both with the broadside direction towards the base station and towards the torso. The figures show the results in both the axes *Tr1* and *Tr2* of Fig. 8. In this case, one can observe that along *Tr1*, the received power remains constant, since no significant fading effect is present due to the high terminal antenna directivity, and it is equal to the one evaluated via the Friis LOS formula. However, when the Airy pattern points towards the torso, as shown in the same figure, the received power is drastically reduced. A similar effect occurs at the beginning of the *Tr2* axis, when the terminal antenna is located in the shadow region, see Fig. 8.

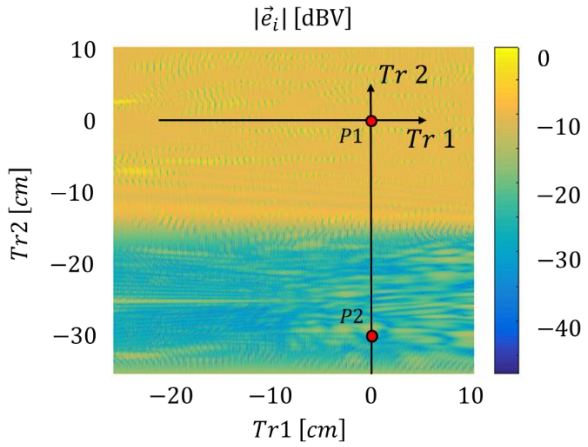

Fig.9 Incident field magnitude map at 120 GHz. The axes Tr1 and Tr2 are shown for the sake of completeness.

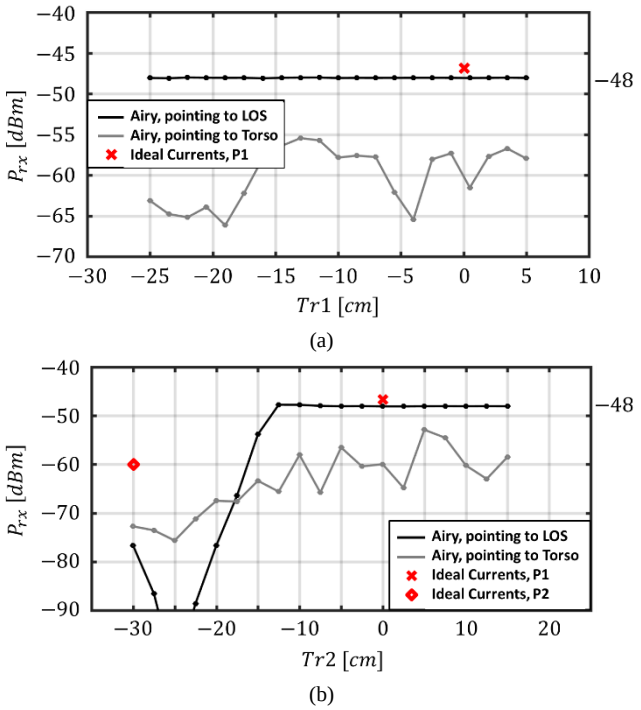

Fig.10 Power received by the 120GHz antenna terminal as a function of its position along the two axes of Fig.8: a) Tr1 and b) Tr2. The red cross and square symbols indicate the available power given by the proposed Observable Field procedure in P_1 and P_2, respectively.

V MULTIPATH DRIVER ANTENNA BEAMFORMING

To improve the coverage, the availability of a terminal antenna pattern with dynamic beam forming capabilities would be a great advantage. This is mostly possible at high frequencies where the terminal antennas can be made electrically large. In this case, the terminal's beam pattern can be changed by dynamically tuning amplitude and phase of the received signals with a coherent array of antennas. To maximize the received power, the array elements weights should be fine-tuned to synthesize the pattern radiated by the ideal currents.

For the stadium scenario presented in Section IV, the Observable Field, and its associated available power, have been calculated in two relevant points, shown in Fig.8: P_1, where the LOS field is dominant, and P_2 located within the shadow region. It is worth noting that the Observable Field is independent of the terminal orientation inside the antenna domain. For the sake of simplicity, let us consider a spherical volume of radius $3.5mm$ to evaluate the available power.

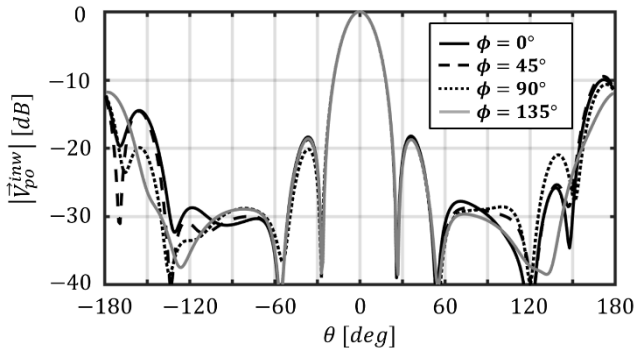

Fig.11 Normalized magnitude of the inward component of the Observable Field's pattern for four different ϕ cuts in P1

Fig. 11 shows the inward component of the Observable Field calculated via the ideal currents procedure described in Section II, associated to an antenna domain S_a, centered in P_1. The pattern in Fig. 11 has two main beams: one along the direction of the LOS incident wave; the other, essentially due to the reflection from the torso, pointing at the user ($\theta = 180°$). The antenna should have a pattern as the one radiated by the ideal currents to receive the maximum power. Moreover, the pattern should change dynamically as function of the terminal location. The realization of this type of antenna is out the scope of this work, and maybe limited by practical considerations.

The available power in P1 results $P_{ava,P1} = -47.2$ dBm, only 1 dB greater than the one calculated with an Airy pattern, see Fig. 10. This increment in the available power is due to the coherent sum of the LOS beam and the one associated to the field reflected by the torso, which is 10 dB lower. Therefore, for $a \approx 1.4\,\lambda$ @ 120 GHz, if the terminal is in a region where the incident field is dominated by the LOS, the required dynamic beam forming should essentially steer an Airy beam towards the LOS, and the torso contribution can be effectively neglected.

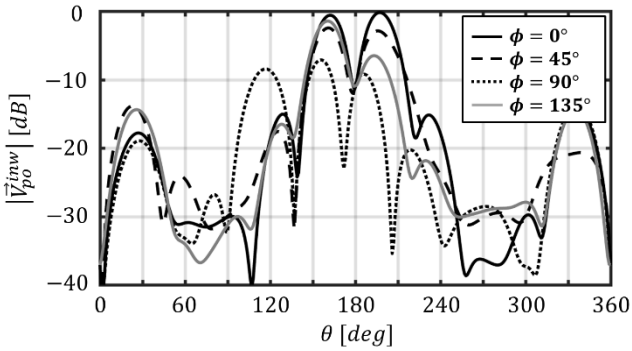

Fig.12 Normalized magnitude of the inward component of the Observable Field's pattern for four different ϕ cuts in P2 at $f_2 = 120$ GHz. Note that to highlight the beam splitting around $\theta = 180°$ the field is plotted for θ varing from 0° to 360°.

Fig.12 shows the inward component of the Observable Field associated to the same antenna domain centered in P_2. Since the scatterers' and their roughness' dimensions are not negligible in terms of wavelength, the interference pattern created by the LOS, and the scattered field is complex. For the considered example, it is apparent that the main contribution is given by the scattering from the torso, and it is located around $\theta = 180°$. It is worth noting that there is a split in this main beam due to the torso roughness. A secondary contribution comes from the LOS direction, $\theta = 0°$, and it is due to the field scattered by the head of the spectator sitting in front of the user under analysis. The pattern of the Ideal antenna is, in this example, quite different from an Airy pattern.

The estimated power available in P2 is $P_{ava,P2} = -60$ dBm, which is much higher than the one achieved by the terminal antenna described in the previous section (Airy Pattern), which was only -76 dBm when pointing to the torso and -83 dBm, when pointing to the base station, as shown in Fig. 10. Therefore, in case of LOS blockage the field scattered by the users can be received to improve the connection to the base station [15]. In this case, the terminal antenna should have not only dynamic steering, but also shaping abilities.

For the sake of completeness Fig. 13 shows the magnitude and phase of the PWS (see Appendix A) of the incident field used to derive the Observable Field in the two previous examples at high frequencies. The PWS is evaluated on a sphere, S_f, of radius $R_f = 3\text{cm}$ enclosing the antenna domain, see Fig. 8. Figs. 13a and 13b show the PWS when the receiver is located in P1. In this case, it presents a stationary phase point in the top sphere around $\theta = 0°$. Thus, the LOS field will be the dominant contribution to the integral in (7) and (8). Therefore, the relevant ideal currents shown in Fig.16a resemble those obtained for a single plane wave coming from $\theta = 0°$ (see Fig. 4a). Hence, the inward component of the Observable Field will be similar to that of an Airy pattern, as shown in Fig. 11. In P_2, the main contribution is instead given by the field scattered from the torso, since the magnitude in the bottom sphere is close to the maximum, and around $\theta = 180°$ the phase is not highly oscillating. However, there is not a clear stationary phase point since the field scattered by a rough surface does not have a predominant direction of propagation. The ideal currents relevant to this case are shown in Fig. 14b. The current distribution is clearly different from that associated to an Airy pattern of Fig. 4a.

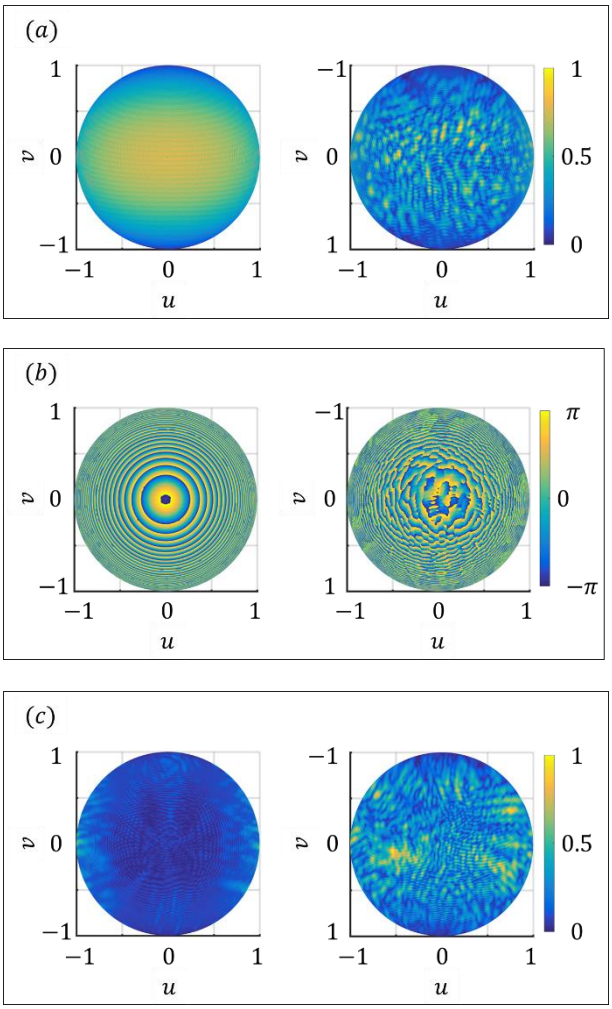

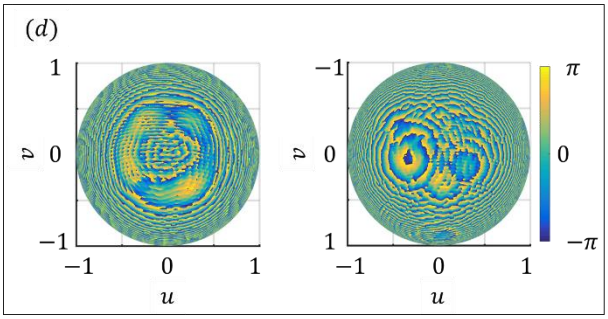

Fig.13 Normalized magnitude (a), (c) and phase (b), (d) of the y component of the PWS of the incident electric field for $f_2 = 120$ GHz when the terminal antenna is located in P_1 (a) and (b), or in P_2 (c) and (d). Top and bottom hemispheres are shown on the left and right, respectively.

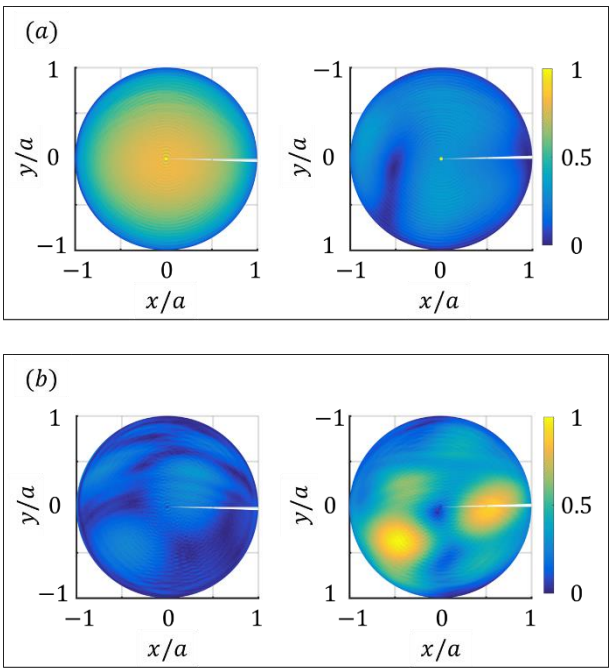

Fig.14 Normalized magnitude of the y-component of the ideal electric currents at 120 GHz when the antenna is located in P_1 (a), and P_2 (b). Top and bottom hemispheres are shown on the left and right, respectively.

Spectral Bandwidth

In this section, the observable field is investigated over a 10 GHz bandwidth, which is wider than the spatial channels proposed in the 120 GHz scenario of [15]. The proposed procedure is applied to different incident fields evaluated with the field transmitted by the base station varying now from 115 GHz to 125 GHz, while keeping the same base station directivity. The inward component of the Observable Field at the extremes of the band is shown in Fig.15. It can be seen that even if small variations on the level of the multiple lobes are present, the shape of the ideal pattern is very similar. Therefore, the available power remains basically the same over the considered bandwidth, as shown in Fig.16. To be more realistic, we have also considered the case where the terminal antenna is in P_2, and its pattern does not change over the considered spectral band, *i.e.* it is frequency independent: fig.16 plots the received power by a terminal antenna with a frequency independent radiation pattern equal to the one of the Observable Field at 120 GHz, shown in Fig.12. The received power is lower than that of the ideal terminal antenna in this case but remains within a 1.5 dB difference.

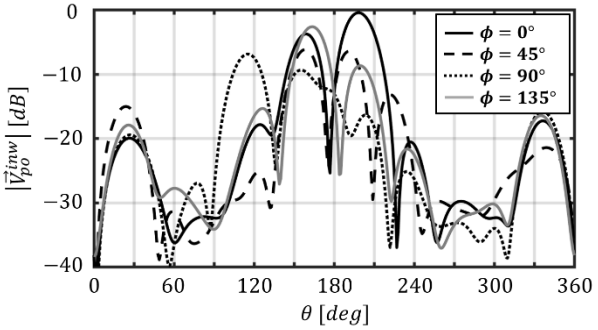

(a)

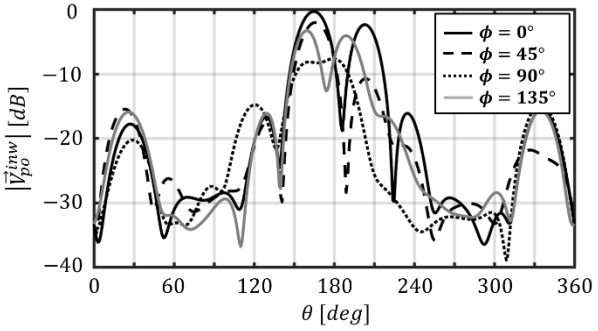

(b)

Fig.15 Normalized magnitude of the inward component of the Observable Field's pattern for four different ϕ cuts in P2 at $f = 115$ GHz (a) and $f = 125$ GHz (b). Note that to highlight the beam splitting around $\theta = 180°$ the field is plotted for θ varing from 0° to 360°.

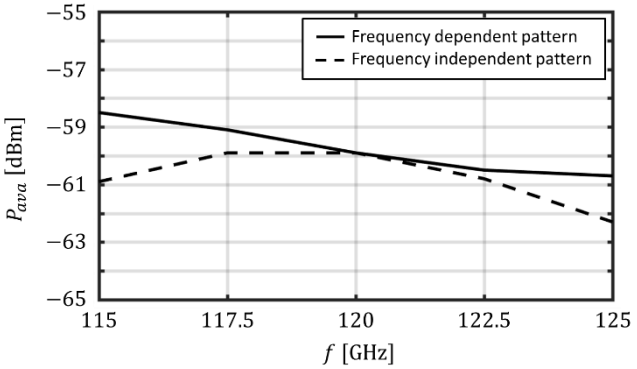

Fig.16 available power as a function of the frequency in case of an ideal terminal antenna in P_2 with a frequency dependent radiation pattern (solid black line), or with a frequency independent radiation pattern (dotted black line).

VI CONCLUSIONS

The Observable Field represents the portion of an arbitrary incident field that an ideal antenna, allocated in certain volume, can receive. Specifically, the ideal antenna operated in reception should scatter a field that is equal and opposite to the outward propagating wave portion of the Observable Field, so that the inward propagating portion is entirely absorbed. In this contribution, we propose an operative procedure to approximate the Observable Field for generalized incidence cases: we choose the outward component of the Observable Field to have an angular distribution that is equal to the Physical Optics (PO) field radiated by equivalent currents defined on the truncated surface of the antenna domain. The amplitude of the observable field is instead obtained by exploiting reciprocity theorem to project the incident field onto the PO field.

The Observable Field concept is then proposed as tool to synthesize the beam which maximizes the power received by antennas illuminated by arbitrary fields. The procedure is applicable to any field but is especially beneficial in environments where the incident field is composed of multiple coherent planes waves, such as those present in communication scenarios where the receiver is located close to multiple scatterers. In such situations, the knowledge of the amplitude, the phase, and the direction of incidence of the different contributions can be used to fine-tune the design of the receiving antenna pattern. The actual design and realization of such antennas is, however, out of the scope of the paper.

APPENDIX A: PLANE WAVE SPECTRUM

The aim of this appendix is to propose a procedure to derive a homogeneous plane wave expansion of a general incident field, valid in the surrounding of a chosen origin. The proposed procedure relies only on the knowledge of the incident field on a sphere of radius R_f centered in the origin.

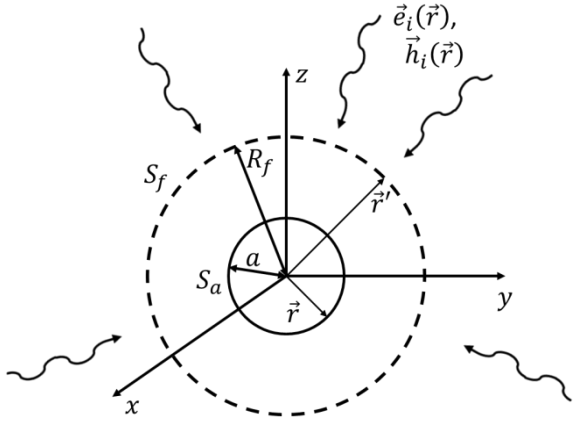

Fig.A1 Geometry of the problem.

Resorting to the equivalence theorem, the electric field inside S_f can be expressed as the radiation integral due to the equivalent currents:

$$\vec{J}_{eq}(\vec{r}') = -\hat{r}' \times \vec{h}_i(\vec{r}'), \quad \text{(A1)}$$

$$\vec{m}_{eq}(\vec{r}') = \hat{r}' \times \vec{e}_i(\vec{r}') \quad \text{(A2)}$$

with $|\vec{r}'| = R_f$.

Thus, the electric field can be expressed as the sum of the contributions due to the equivalent electric and magnetic currents, i.e. $\vec{e}_i(\vec{r}) = \vec{e}_i^{\,j}(\vec{r}) + \vec{e}_i^{\,m}(\vec{r})$. Each contribution can be evaluated resorting to the dyadic Green's function of an unbounded homogeneous medium as follows:

$$\vec{e}_i^{\,j}(\vec{r}) = -j\omega\mu \iint_{S_f} \left(\bar{\bar{I}} + \frac{\vec{\nabla}\vec{\nabla}}{k^2}\right) \frac{e^{-jk|\vec{r}-\vec{r}'|}}{4\pi|\vec{r}-\vec{r}'|} \cdot \vec{J}_{eq}(\vec{r}')d\vec{r}', \quad \text{(A3)}$$

$$\vec{e}_i^{\,m}(\vec{r}) = -\iint_{S_f} \vec{\nabla} \frac{e^{-jk|\vec{r}-\vec{r}'|}}{4\pi|\vec{r}-\vec{r}'|} \times \vec{m}_{eq}(\vec{r}')d\vec{r}'. \quad \text{(A4)}$$

By making use of the addition Theorem for the Legendre Polynomials (§7.5 of [22]) we obtain:

$$\frac{e^{-jk|\vec{r}'-\vec{r}|}}{4\pi|\vec{r}'-\vec{r}|} \equiv -\frac{jk}{4\pi} \oiint_U e^{j\vec{k}_q\cdot\vec{r}} T_L(\vec{k}_q, \vec{r}')d\hat{k}_q\,, \quad \text{(A5)}$$

where U is the unit sphere (*i.e.* the Ewald sphere), $d\hat{k}_q = sin\alpha d\alpha d\beta$, and the translation operator:

$$T_L\left(\hat{k}_q, \vec{r}'\right) = \sum_{l=0}^{L}(-j)^l(2l+1)h_l^{(2)}(kr')P_l\left(\hat{r}\cdot\hat{k}_q\right), \quad \text{(A6)}$$

being P_l the Legendre polynomial, and $h_l^{(2)}$ the spherical Hankel function of the second kind of order l. The previous expression can be rewritten as superposition of homogeneous plane waves, as follows:

$$\vec{e}_i^{\,j}(\vec{r}) = -\frac{\zeta k^2}{(4\pi)^2}\iint_U\left(\bar{\bar{I}} - \hat{k}_q\hat{k}_q\right)\cdot\vec{\bar{S}}_L\left(\vec{k}_q\right)e^{j\vec{k}_q\vec{r}}d\hat{k}_q\,, \quad \text{(A7)}$$

$$\vec{e}_i^{\,m}(\vec{r}) = -\frac{k^2}{(4\pi)^2}\iint_U\ \hat{k}_q\times\vec{\bar{Q}}_L\left(\vec{k}_q\right)e^{j\vec{k}_q\vec{r}}d\hat{k}_q\,, \quad \text{(A8)}$$

where $\vec{\bar{S}}_L\left(\vec{k}_q\right) = \iint_{S_f}\ T_L\left(\hat{k}_q,\vec{r}'\right)\vec{J}_{eq}(\vec{r}')d\vec{r}'$, and $\vec{\bar{Q}}_L\left(\vec{k}_q\right) = \iint_{S_f}\ T_L\left(\hat{k}_q,\vec{r}'\right)\vec{m}_{eq}(\vec{r}')d\vec{r}'$.

It is worth noting that for $kR_f \gg 1$ the translation operator goes to $T_L\left(\hat{k}_q,\vec{r}'\right) \to j4\pi\frac{e^{-jkR_f}}{kR_f}\delta\left(\hat{r}'\cdot\hat{k}_q\right)$ and

$$\vec{e}_i^{\,j}(\vec{r}) \simeq -jk\zeta\frac{e^{-jkR_f}}{4\pi R_f}\int_0^{2\pi}\int_0^{\pi}\ \left(\bar{\bar{I}} - \hat{r}'\hat{r}'\right)\cdot\vec{J}_{eq}(\vec{r}')e^{j\vec{r}\cdot\vec{r}'}d\vec{r}'\,, \quad \text{(A9)}$$

$$\vec{e}_i^{\,m}(\vec{r}) \simeq -jk\frac{e^{-jkR_f}}{4\pi R_f}\int_0^{2\pi}\int_0^{\pi}\ \hat{r}'\times\vec{m}_{eq}(\vec{r}')e^{j\vec{r}\cdot\vec{r}'}d\vec{r}'. \quad \text{(A10)}$$

The expressions (A9), (A10) are valid only in a limited region surrounding the origin. The limiting radius r_a^{MAX} of this region can be evaluated assuming a 10% error in amplitude, and $\pi/8$ in phase, as described in [23], so that:

$$r_a^{max} = min\left(0.1R_f, \sqrt{\frac{R_f\lambda_0}{8}}\right) \quad \text{(A11)}$$

This equation implies that (A9) and (A10) can be used evaluating the field on a sphere located in the far field of the antenna domain. In this case the evaluation of the field spectrum is straightforward.

In order to achieve a single integral representation for the electric field such that it accounts for both the electric and magnetic currents, equations (A9) and (A10) can be summed up, eventually obtaining:

$$\vec{e}_i(\vec{r}_a) = \int_0^{2\pi}\int_0^{\pi}\ \vec{E}^{\,pws}\left(-\hat{k}_i\right)e^{jk\vec{r}_a\cdot\hat{k}_i}\,d\hat{k}_i\,, \quad \text{(A12)}$$

where we applied the change of variable $\hat{k}_i = \hat{r}'$, and

$$\vec{E}^{pws}\left(-\hat{k}_i\right) = -jkR_f\frac{e^{-jkR_f}}{4\pi}\{-\hat{k}_i\times\zeta\vec{h}_i\left(R_f\hat{k}_i\right) + \hat{k}_i\times[\hat{k}_i\times\vec{e}_i\left(R_f\hat{k}_i\right)]\}\,. \quad \text{(A13)}$$

Similarly, the spectrum of the magnetic field around the origin can be approximated in terms of the incident electric and magnetic fields, as follows:

$$\vec{h}_i(\vec{r}_a) = \frac{1}{\zeta}\int_0^{2\pi}\int_0^{\pi} -\hat{k}_i\times\ \vec{E}^{\,pws}\left(-\hat{k}_i\right)e^{jk\vec{r}_a\cdot\hat{k}_i}\,d\hat{k}_i\,. \quad \text{(A14)}$$

APPENDIX B: EVALUATION OF THE AMPLITUDE OF THE OBSERVABLE FIELD

The evaluation of the amplitude C of the Observable Field in (9) is expressed as a field reaction. This reaction is set as follows: the incident electric and magnetic fields are first expressed using the observable and the remaining fields, as in (1):

$$\vec{f}_i(\vec{r}_\infty) = C\vec{f}_{po}(\vec{r}_\infty) + \vec{f}_{rem}(\vec{r}_\infty)\,. \quad \text{(B1)}$$

Then, both the LHS and the RHS of (B1) are multiplied with a field test function $\vec{f}_t(\vec{r}_\infty)$, and integrated over a sphere S_∞ in the far field of the antenna domain, as follows:

$$< \vec{f}_i, \vec{f}_t > = C < \vec{f}_{po}, \vec{f}_t > + < \vec{f}_{rem}, \vec{f}_t > \quad \text{(B2)}$$

where the reaction integral $\langle \vec{f}_i,\ \vec{f}_t\rangle$ is defined as in (10).

An appropriate choice for the test function is here introduced as the fields radiated by the ideal antenna when operated in transmission: $\vec{e}_t(\vec{r}_\infty) = \vec{e}_{tx}(\vec{r}_\infty)$, $\vec{h}_t(\vec{r}_\infty) = \vec{h}_{tx}(\vec{r}_\infty)$. The fields $\vec{f}_{tx}$ radiated by the ideal can be expressed as those radiated by a set of equivalent currents defined over the antenna domain $\vec{J}_{tx}(\vec{r}_a), \vec{m}_{tx}(\vec{r}_a)$. These currents are related to those describing the inward component of the Observable Field as follows:

$$\vec{J}_{tx}(\vec{r}_a) = -\vec{J}_{po}^{\,*}(\vec{r}_a)\,, \quad \text{(B3a)}$$

$$\vec{m}_{tx}(\vec{r}_a) = \vec{m}_{po}^{\,*}(\vec{r}_a)\,. \quad \text{(B3b)}$$

Therefore, the angular distribution of the fields radiated by the antenna in transmission can be related to those of the Observable Field by the antenna in reception, as follows:

$$\vec{e}_{tx}(\vec{r}_\infty) = \vec{V}_{po}^{\,inw*}\left(\hat{k}\right)\frac{e^{-jkr_\infty}}{r_\infty}\,, \quad \text{(B4a)}$$

$$\vec{h}_{tx}(\vec{r}_\infty) = \frac{1}{\zeta}\hat{k}\times\vec{e}_{tx}(\vec{r}_\infty)\,. \quad \text{(B4b)}$$

The value of the constant C can then be obtained by solving (B2). By considering that the reaction between the remaining and the antenna angular distribution (B4) can be approximated to be zero $< \vec{f}_{rem}, \vec{f}_{tx} > \approx 0$. This is because the remaining and Observable Fields are basically orthogonal, $< \vec{f}_{rem}, \vec{f}_{po} > \approx 0$, similar to the expansion of low and high order spherical modes as clarified in [7]. The fields radiated by the antenna have the same orthogonality property with the remaining field since they have the same angular distribution as the Observable Field, (B4). With this approximation it follows that:

$$C \approx \frac{\langle\vec{f}_i,\vec{f}_{tx}\rangle}{\langle\vec{f}_{po},\vec{f}_{tx}\rangle}\,. \quad \text{(B5)}$$

It is worth noting that the denominator in (B5) can be related to the radiated power by the ideal antenna in transmission. In fact, expanding the angular distribution of the observable field in inward and outward components, $\vec{f}_{po} = \vec{f}_{po}^{\,inw} + \vec{f}_{po}^{\,outw}$, one can easily demonstrate that $\langle\vec{f}_{po}^{\,outw},\vec{f}_{tx}\rangle = 0$, and thus

$$\langle \vec{f}_{po}, \vec{f}_{tx} \rangle = \langle \vec{f}_{po}^{inw}, \vec{f}_{tx} \rangle = 4P_{rad}^{tx} \quad \text{(B6)}$$

where P_{rad}^{tx} is the power radiated by the currents in (B3), i.e. $I_0 = 1$.

ACKNOWLEDGEMENT

This work has been supported by the ERC starting grant Lens Antenna Arrays for Coherent THz Cameras (LAA-THz-CC, 639749)

REFERENCES

[1] I. Liberal and R. W. Ziolkowski, "Analytical and Equivalent Circuit Models to Elucidate Power Balance in Scattering Problems," *IEEE Trans. Antennas Propagat.*, vol. 61, no. 5, pp. 2714-2726, May 2013.

[2] J. B. Andersen and A. Frandsen, "Absorption Efficiency of Receiving Antennas," *IEEE Trans. Antennas Propag.*, vol. 53, no. 9, pp. 2843-2849, Sep 2005.

[3] H. Shannan and R. Kastner, "On the Incident Power on a Receiving Slender Antenna and the Optical Theorem in the Near Field," *IEEE Trans. Antennas Propagat.*, vol. 65, no. 5, pp. 2421-2427, May 2017.

[4] L. Brillouin, "The Scattering Cross Section of Spheres for Electromagnetic Waves," *Journal of Applied Physics*, 20, 1110 (1949); doi: 10.1063/1.1698280

[5] K. Do-Hoon, D.M. Pozar, "Optimal Characteristics of an Arbitrary Receive Antenna," *IEEE Trans. Antennas Propag.*, vol. 57, no. 12, pp. 3720-3727, Dec. 2009.

[6] P.S. Kildal, E. Martini, S. Maci, "Degrees of Freedom and Maximum Directivity of Antennas: a bound on maximum directivity of nonsuperreactive antennas," *IEEE Trans. Antennas Propag*., vol. 59, no. 4, pp. 16-25, Aug 2017.

[7] A. Neto, N. Llombart, A.Freni: "The Observable Field for Antennas in Reception," *IEEE Trans. Antennas Propag.,* vol. 66, no. 4, pp. 1736-1746, Apr 2018.

[8] T. S. Rappaport et al., "Millimeter wave mobile communications for 5G cellular: It will work!," *IEEE Access*, vol. 1, pp. 335–349, May 2013.

[9] B. Xu, Z. Ying, L. Scialacqua, A. Scannavini, L. J. Foged, T. Bolin, K. Zhao, S. He, M. Gustafsson. "Radiation Performance Analysis of 28 GHz Antennas Integrated in 5G Mobile Terminal Housing," *IEEE Access*, vol. 6, pp. 48088 – 48101, Aug 2018.

[10] W. Hong, "Solving the 5G mobile antenna puzzle: assessing future directions for the 5G mobile antenna paradigm shift," *IEEE microwave magazine*, vol. 18, no. 7, pp. 86 – 102, Dec 2017.

[11] S. Zhang, X. Chen, I. Syrytsin, G. F. Pedersen, "A Planar Switchable 3-D-Coverage Phased Array Antenna and Its User Effects for 28-GHz Mobile Terminal Applications," *IEEE Trans. Antennas Propag.*, vol. 65, no. 12, pp. 6413 – 6421, Dec 2017.

[12] I. Syrytsin, S. Zhang, G. F. Pedersen, A. S. Morris, "Compact Quad-mode planar phased array with wideband for 5G mobile terminals," in *IEEE Trans. Antennas Propag.*, vol. 66, no. 9, pp. 4648 – 4657, Sep 2017.

[13] W. Roh, J. Seol, J. Park, B. Lee, J. Lee, Y. Kim, J. Cho, K. Cheun, F. Aryanfar, "Millimeter-wave beamforming as an enabling technology for 5G cellular communications: theoretical feasibility and prototype results," *IEEE communications magazine*, vol. 52, no. 2, pp. 106 – 113, Feb 2014.

[14] M. K. Samimi, T. S. Rappaport, "Ultra-Wideband Statistical Channel Model for Non Line of Sight Millimeter-Wave Urban Channels," *IEEE Global Communications Conference* (GLOBECOM), 2014

[15] N. Llombart et al. "Fly's Eye Spherical Antenna System for Future Tbps Wireless Communications," *11th EuCAP*, Paris, France, 2017.

[16] V. Rumsey, "On the design and performance of feeds for correcting spherical aberration," *IEEE Trans. Antennas Propag.*, vol. 18, no. 3, pp. 343-351, May 1970.

[17] A.T. De Hoop, *The n-port receiving antenna and its equivalent electrical network*, Technical Report, Philips Res. Rep., 30, 302–315, 1975.

[18] T. Wu, T. S. Rappaport and C. M. Collins, "The human body and millimeter-wave wireless communication systems: Interactions and implications," *2015 IEEE International Conference on Communications (ICC)*, London, pp. 2423-2429, 2015.

[19] GRASP 10.5.0, [Online] Available: http://www.ticra.com/software/grasp

[20] P. F. M. Smulders, "Statistical Characterization of 60-GHz Indoor Radio Channels", *IEEE Trans. Antennas Propag.*, vol. 57, no. 10, pp. 2820-2829, Oct. 2009.

[21] Yi Chen and Dirk Manteuffel, "A Tunable Decoupling and Matching Concept for Compact Mobile Terminal Antennas," *IEEE Trans. Antennas Propag.*, vol. 65, no. 4, pp. 1570 – 1578, Feb 2017.

[22] J. A. Stratton, *Electromagnetic Theory*, IEEE Press Series on Electromagnetic Wave Theory, Wiley-Interscience, 2007.

[23] N. Llombart, B. Blazquez, A. Freni, A. Neto, "Fourier Optics for the Analysis of Distributed Absorbers Under THz Focusing Systems," *IEEE Trans. THz Sci. Technol.*, vol.5, no.4, pp.573-583, Jul 2015.

Andrea Neto (M'00 SM'10–F'16) received the Laurea degree (summa cum laude) in electronic engineering from the University of Florence, Florence, Italy, in 1994, and the Ph.D. degree in electromagnetics from the University of Siena, Siena, Italy, in 2000. Part of his Ph.D. degree was developed at the European Space Agency Research and Technology Center Noordwijk, The Netherlands.

He worked for the Antenna Section at the European Space Agency Research and Technology Center for over two years. From 2000 to 2001, he was a Postdoctoral Researcher with the California Institute of Technology, Pasadena, CA, USA, where he worked with the Sub-mm Wave Advanced Technology Group. From 2002 to January 2010, he was a Senior Antenna Scientist with TNO Defence, Security, and Safety, The Hague, The Netherlands. In February 2010, he became a Full Professor of applied electromagnetism with the EEMCS Department, Technical University of Delft, Delft, The Netherlands, where he formed and leads the THz Sensing Group. His research interests include the analysis and design of antennas with an emphasis on arrays, dielectric lens antennas, wideband antennas, EBG structures, and THz antennas.

Dr. Neto served as an Associate Editor of the IEEE TRANSACTIONS ON ANTENNAS AND PROPAGATION (2008–2013) and IEEE ANTENNAS AND WIRELESS PROPAGATION LETTERS (2005–2013). He is a member of the Technical Board of the European School of Antennas and organizer of the course on antenna imaging techniques. He is a member of the Steering Committee of the Network of Excellence NEWFOCUS, dedicated to focusing techniques in mm and sub-mm wave regimes. In 2011, he was the recipient of the European Research Council Starting Grant to perform research on Advanced Antenna Architectures for THz Sensing Systems. He was the recipient of the H. A. Wheeler Award for the best applications paper of 2008 in the IEEE TRANSACTIONS ON ANTENNAS AND PROPAGATION, the Best Innovative Paper Prize of the 30th ESA Antenna Workshop in 2008, and the Best Antenna Theory Paper Prize of the European Conference on Antennas and Propagation (EuCAP) in 2010. In 2011, he was the recipient of the European Research Council Starting Grant to perform research on advanced antenna architectures for THz sensing systems.

Arturo Fiorellini Bernardis received his B.Sc. in biomedical engineering from the Politecnico di Milano, Italy, in 2014, and the M.Sc. degree (cum laude) in electrical engineering from the Delft University of Technology (TU Delft), The Netherlands, in 2017. He is currently a Ph.D. candidate at the Terahertz Sensing Group, Department of Microelectronics, TU Delft. His research interests include electromagnetic theory as well as the analysis and design of photoconductive antennas for security applications.

Diego Emer received his B. Sc. in telecommunication engineering in 2014 from the Politechnico di Milano, Italy. In 2018 he completed his master's degree in electrical engineering at Delft University of Technology, The Netherlands, writing his thesis in the Terahertz Sensing Group, Department of Microelectronics. He is currently working as network planning engineer

Angelo Freni (S'90-M'91-SM'03) received the Laurea (Doctors) degree in Electronics Engineering from the University of Florence in 1987. Since 1990 he is with the Department of Electronic Engineering of the University of Florence, Italy, first as Assistant Professor and from 2002 as Associate Professor of electromagnetism; in 2014 he obtained the Full Professor qualification. From 1995 to 1999 he has also been an Adjunct Professor at the University of Pisa, and from 2012 a Visiting Professor at the TU Delft University of Technology, Delft, The Netherlands. During 1994, he was involved in research at the Engineering Department of the University of Cambridge, UK, concerning the extension and the application of the finite element method to the electromagnetic scattering from periodic structures. Between 2009 and 2010 he also spent one year as a researcher at the TNO Defence, Security and Safety, The Hague, The Netherlands, working on the electromagnetic modeling of kinetic inductance devices and their coupling with array of slots in THz range. His research interests include meteorological radar systems, radiowave propagation, numerical and asymptotic methods in electromagnetic scattering and antenna problems, electromagnetic interaction with moving media and remote sensing. In particular, part of his research concerned numerical techniques based on the integral-equation, with focus on domain-decomposition and fast solution methods.

Nuria Llombart (S'06–M'07–SM'13) received the Master's degree in electrical engineering and Ph.D. degrees from the Polytechnic University of Valencia, Valencia, Spain, in 2002 and 2006, respectively.

During her Master's degree studies, she spent one year at the Friedrich-Alexander University of Erlangen-Nuremberg, Erlangen, Germany, and worked at the Fraunhofer Institute for Integrated Circuits, Erlangen, Germany. From 2002 to 2007, she was with the Antenna Group, TNO Defense, Security and Safety Institute, The Hague, The Netherlands, working as a Ph.D. student and afterwards as a Researcher. From 2007 to 2010, she was a Postdoctoral Fellow with the California Institute of Technology, working with the Submillimeter Wave Advance Technology Group, Jet Propulsion Laboratory, Pasadena, CA, USA. She was a "Ramón y Cajal" fellow in the Optics Department, Complutense University of Madrid, Madrid, Spain, from 2010 to 2012. In September 2012, she joined the THz Sensing Group, Technical University of Delft, Delft, The Netherlands. In February 2018 she became Full Professor. She has coauthored more than 150 journal and international conference contributions. Her research interests include the analysis and design of planar antennas, periodic structures, reflector antennas, lens antennas, and waveguide structures, with emphasis in the THz range.

Dr. Llombart was the recipient H. A. Wheeler Award for the Best Applications Paper of 2008 in the IEEE TRANSACTIONS ON ANTENNAS AND PROPAGATION, the 2014 THZ SCIENCE AND TECHNOLOGY Best Paper Award of the IEEE Microwave Theory and Techniques Society, and several NASA awards. She was also the recipient of the 2014 IEEE Antenna and Propagation Society Lot Shafai Mid-Career Distinguished Achievement Award. She serves as a Board member of the IRMMW-THz International Society. In 2015, she was the recipient of European Research Council Starting Grant.